ORIGINAL ARTICLE

Prediction of oxygen supplementation by a deep-learning model integrating clinical parameters and chest CT images in COVID-19

Naoko Kawata[1,2,3] · Yuma Iwao[4,5] · Yukiko Matsuura[6] · Masaki Suzuki[7] · Ryogo Ema[8] · Yuki Sekiguchi[2] · Hirotaka Sato[1,9] · Akira Nishiyama[10] · Masaru Nagayoshi[6] · Yasuo Takiguchi[6] · Takuji Suzuki[1] · Hideaki Haneishi[4]

Abstract

Purpose As of March 2023, the number of patients with COVID-19 worldwide is declining, but the early diagnosis of patients requiring inpatient treatment and the appropriate allocation of limited healthcare resources remain unresolved issues. In this study we constructed a deep-learning (DL) model to predict the need for oxygen supplementation using clinical information and chest CT images of patients with COVID-19.

Materials and methods We retrospectively enrolled 738 patients with COVID-19 for whom clinical information (patient background, clinical symptoms, and blood test findings) was available and chest CT imaging was performed. The initial data set was divided into 591 training and 147 evaluation data. We developed a DL model that predicted oxygen supplementation by integrating clinical information and CT images. The model was validated at two other facilities (n = 191 and n = 230). In addition, the importance of clinical information for prediction was assessed.

Results The proposed DL model showed an area under the curve (AUC) of 89.9% for predicting oxygen supplementation. Validation from the two other facilities showed an AUC > 80%. With respect to interpretation of the model, the contribution of dyspnea and the lactate dehydrogenase level was higher in the model.

Conclusions The DL model integrating clinical information and chest CT images had high predictive accuracy. DL-based prediction of disease severity might be helpful in the clinical management of patients with COVID-19.

Keywords COVID-19 · Disease severity prediction · Chest CT images · Deep learning · Explainable AI

Abbreviations

AG ratio	Albumin:globulin ratio
ALB	Albumin
ALT	Alanine aminotransferase
AST	Aspartate aminotransferase
AUC	Area under the receiver operating characteristic curve
Baso	Basophil
BMI	Body mass index
BUN	Blood urea nitrogen
Cl	Chloride ion
COPD	Chronic obstructive pulmonary disease
COVID-19	Coronavirus disease 2019
CPK	Creatine phosphokinase
Cre	Creatinine
CRP	C-reactive protein
DL	Deep learning
ECMO	Extracorporeal membrane oxygenation
eGFR	Estimated glomerular filtration rate
Eosino	Eosinophil
GLU	Glucose
Grad-Cam	Gradient-weighted class activation mapping
Hct	Hematocrit
HFNC	High-flow nasal canula
HGB	Hemoglobin
K	Potassium
KL-6	Sialylated carbohydrate antigen
LDH	Lactate dehydrogenase
LIME	Local interpretable model-agnostic explanations
Lympho	Lymphocyte
MCH	Mean corpuscular hemoglobin
MCHC	Mean corpuscular hemoglobin concentration
MCV	Mean corpuscular volume

Naoko Kawata and Yuma Iwao contributes equally to this work.

Extended author information available on the last page of the article

Mono	Monocyte
Na	Sodium
NA	Not assessed
Neutro	Neutrophil
PLT	Platelet
PNI	Prognostic nutritional index
RBC	Red blood cell
RT-PCR	Real-time reverse transcriptase chain reaction
SARS-CoV-2	Severe acute respiratory syndrome coronavirus 2
T-Bil	Total bilirubin
TP	Total protein
UA	Uric acid
WBC	White blood cell

Introduction

The pandemic of the coronavirus disease 2019 (COVID-19) has caused > 750 million infections and 6.8 million deaths worldwide as of 1 March 2023 [1]. The overall trend in infections is downward, but there are still no signs of disease eradication. Rapid and effective triage also remains an unresolved issue for optimal treatment and effective allocation of limited healthcare resources [2].

The viral nucleic acid real-time reverse transcriptase chain reaction (RT-PCR) is the gold standard for the diagnosis of COVID-19 infection [3, 4]. RT-PCR has several limitations, however, such as dependence of the diagnosis on the viral load and sampling technique [5]. With the rapid increase in the number of cases, there are problems regarding the time required for testing and the lack of reagents. Furthermore, challenges remain, including the diagnosis of severe acute respiratory syndrome coronavirus 2 (SARS-CoV-2) pneumonia and determination of disease severity [6].

Numerous studies have shown the utility of chest CT images for the diagnosis of SARS-CoV-2 pneumonia [7–9], even in PCR-negative cases [10]. SARS-CoV-2 pneumonia is characterized by ground glass opacities in the lung parenchyma bilaterally on radiographs [11]; subsequently, infiltrating shadows are apparent. Numerous reports have quantified ground glass opacities, semi-consolidated, and consolidated lesions, and concluded that abnormal lung areas exceeding a specified value are associated with severe disease [12, 13]. Analyses using radiomic features have also been reported [14].

The relationship between COVID-19 disease severity and clinical characteristics has also been reported. Early reports have described the patient characteristics that are associated with severe disease, including older age, gender, obesity, and co-morbidities, such as hypertension, diabetes, chronic lung diseases and coronary artery disease [15–17]. Subsequent reports indicated that coagulopathies and vasculitis contribute to critical illness in patients with COVID-19 [18, 19]. Markers of lung fibrosis, such as sialylated carbohydrate antigen (KL-6), have also been reported to contribute to the progression from pneumonia to secondary lung fibrosis [20].

In parallel, deep learning (DL)-based chest image analysis has been used to predict COVID-19 disease severity, survival, and death [21], with some reports showing a diagnostic accuracy > 80% [22]. A recent study proposed nomograms and scoring systems using DL to determine COVID-19 patient status and predict critical illness [23]. However, a DL model has not been fully described in detail using clinical information and chest images together [24]. It has been recently reported that a DL model using x-rays predicts the presence or absence of oxygen supplementation, a predictor of hospitalization and delayed discharge, which is associated with disease severity [25]. Thus, we considered a DL model that combined clinical and CT imaging findings to predict oxygen supplementation in an early stage. In addition, if we enable visualization of the elements on which the DL model is built, such a DL model will facilitate healthcare professionals' efforts to provide appropriate treatment and allocate healthcare resources in the next pandemic and for other respiratory diseases.

Therefore, we constructed a DL model for predicting oxygen supplementation at an early stage in COVID-19 infection that integrated clinical information and chest CT images.

Methods

Study subjects

To construct the prediction model, we enrolled 819 consecutive COVID-19 patients who were hospitalized and treated at Chiba Aoba Municipal Hospital (No. 20200301) Municipal Hospital from February 2020 to September 2021. The subjects were required to meet all of the following inclusion criteria: (1) Patients with symptoms suspicious for COVID-19 who were diagnosed with COVID-19 during the COVID-19 outbreak; (2) Patients who underwent RT-PCR tests of nasopharyngeal swab samples to establish a COVID-19 diagnosis; and (3) Patients with a positive PCR test result and a request for treatment and hospitalization from the local health department. We excluded subjects under 20 years of age (n = 31), subjects who did not undergo CT scanning (n = 32), data mismatches (n = 14), pregnant patients (n = 3), and a transfer case (n = 1); thus 738 patients were finally enrolled.

External validation was performed at two other facilities. These two medical facilities differ in location, local population, and function as hospitals. The first external validation

included 191 patients with COVID-19 who were admitted and treated at Kashiwa Kousei General Hospital (No. 21005) General Hospital. The second external validation included 230 patients with COVID-19 who were admitted and treated at Eastern Chiba Medical Center (No.161) Medical Center.

This retrospective multi-center study was approved by the Institutional Review Boards of Chiba University (No. 4074), Chiba Aoba Municipal Hospital (No. 20200301), Kashiwa Kousei General Hospital (No. 21005), and Eastern Chiba Medical Center (No.161). The study was conducted in accordance with the principles of the Declaration of Helsinki. The institutional review boards of all hospital institutions included in the present study provided ethical approval. The requirement for written informed consent was waived. To avoid any potential breach of patient confidentiality, the data were deidentified and had no linkage to the researchers.

Clinical information

We obtained data by reviewing patient charts at the time of admission and during hospitalization. Patient background, clinical symptoms, and blood test findings were collected for clinical information. These data were collected within 24 h of the first visit or admission. Patient background included 19 items and clinical symptoms included 9 items. Blood test findings included 34 items [Supplementary Table 1(a) and (b)].

Each item was based on data obtained from at least 80% of patients from the first derivation facility. The total number of items was 62. To construct the DL model, each patient data set was normalized and any missing data were filled in using the mode method.

Chest CT scanning

At the initial facility, the patients underwent chest CT using an 80-row CT scanner (Siemens, Erlangen, Germany). The patients were scanned from the thoracic inlet to the diaphragm during full inspiration without contrast enhancement. The CT settings were as follows: 120 kV; CT-auto exposure control; gantry rotation time, 0.5 s; and beam pitch, 0.83. All images were reconstructed using soft (I40f) and sharp reconstruction kernels (B70f) with a slice thickness of 3 mm and a reconstruction interval of 3 mm.

At the facility for the first validation, the patients underwent chest CT using a 64-row CT scanner (Siemens) and were scanned from the thoracic inlet to the diaphragm during full inspiration without contrast enhancement. The CT settings were as follows: 120 kV; CT-auto exposure control; gantry rotation time, 0.5 s; and beam pitch, 1.2. All images were reconstructed using soft (I31f) and sharp reconstruction kernels (B70f) with a slice thickness of 5 mm and a reconstruction interval of 5 mm.

At the facility for the second validation, the patients underwent chest CT using an 80-row CT scanner (Aquilion ONE; Canon Medical Systems, Otawara, Tochigi, Japan) and were scanned from the thoracic inlet to the diaphragm during full inspiration without contrast enhancement. The CT settings were as follows: 120 kV; CT-auto exposure control; gantry rotation time, 0.5 s; and beam pitch, 0.813. All images were reconstructed using soft (FC03) and sharp reconstruction kernels (FC51) with a slice thickness of 5 mm and a reconstruction interval of 5 mm. In the present study, only the soft reconstruction kernel was used for each model construction. The sharp reconstruction kernel was used for the data confirmation.

Clinical end point

The patients were divided into two groups according to the oxygen requirements during hospitalization. In the present retrospective study, oxygen supplementation was introduced when the following conditions were confirmed: a partial pressure of arterial oxygen ≤ 60 mmHg or oxygen saturation by pulse oximetry (SpO_2) $\leq 93\%$ and the attending physician considered oxygen supplementation necessary, as specified by the Japanese COVID-19 guidelines [26]. An oxygen requirement was defined as 1 and no oxygen requirement was defined as 0.

The Japanese COVID-19 guideline for oxygen supply is an SpO_2 93% as an additional 3% error in measurement to the general standard of an $SpO_2 \leq 90\%$, which reflects a $PaO_2 \leq 60$ mmHg for respiratory failure. Mild disease is an $SpO_2 \geq 96\%$ without respiratory symptoms or no dyspnea with cough only. No findings suggestive of pneumonia were present in any of these cases. Moderate I is an $SpO_2 > 93\%$ but $< 96\%$ with findings of dyspnea and pneumonia and no requirement for oxygenation, but requires careful follow-up in case of deterioration. Moderate II requires oxygen administration with an $SpO_2 \leq 93\%$. Critical illness requires ICU admission or ventilatory management.

Data set

After excluding mismatch data, the data were randomly divided into training and evaluation data sets (4: 1). The total number of the data sets was 738. The number of training data sets was 591 and the number of evaluation data sets was 147. For the first external validation, the test data set was 191. For the second external validation, the data set was 230.

DL model

In this study we created three DL models and compared the prediction accuracies. The first DL model was designated the clinical network architecture, which used clinical

information (Fig. 1(a)). The clinical information (patient background, symptoms, and blood test findings; n = 62 items) was reformed into 62 channels, convo-transposed twice, and passed through a fully connected layer to generate outputs (1 for oxygen supplementation; 0 for no oxygen supplementation).

The second DL model was designated the image network architecture, referring to previous reports based on DenseNet [22, 27]. The image network architecture model was implemented using chest CT images (Fig. 1(b)). Chest CT images were trimmed around the lungs and resized to $320 \times 200 \times 150$ pixels. After passing through the convolution layer, the model passed through three transitions: dense block, convolution layer, and average pooling. Then, after going through global average pooling, the model passed through the fully connected layer to produce the output.

The third model combined the clinical and image network architectures, and was designated the proposed network architecture (Fig. 2). Referring to the transfer learning method [28], the clinical network block generated by the clinical network architecture and the image network block generated by the image network architecture were fixed

based on the optimal parameters, respectively. Then the clinical and image network blocks were combined and passed through ResNet [29], and finally through a fully connected layer. Only the parameters in the layers after ResNet were updated by learning. Then, the final output was generated.

The learning environment was as follows: the number of epochs was 20; the loss function was binary cross-entropy; the optimization method was Adam; and the learning rate was 0.001.

Analysis of factors affecting the prediction of oxygen supplementation

As an additional validation, we evaluated the importance of each clinical datum. To interpret DL models, gradient-weighted class activation mapping (Grad-Cam) for the image input [30] and local interpretable model-agnostic (LIME) were used for the table data [31]. Of note, there is no general analysis method to identify the contribution of methods that combine CT images and clinical information, such as the model we created. Hence, we evaluated the importance of each item using the following formula, where M is
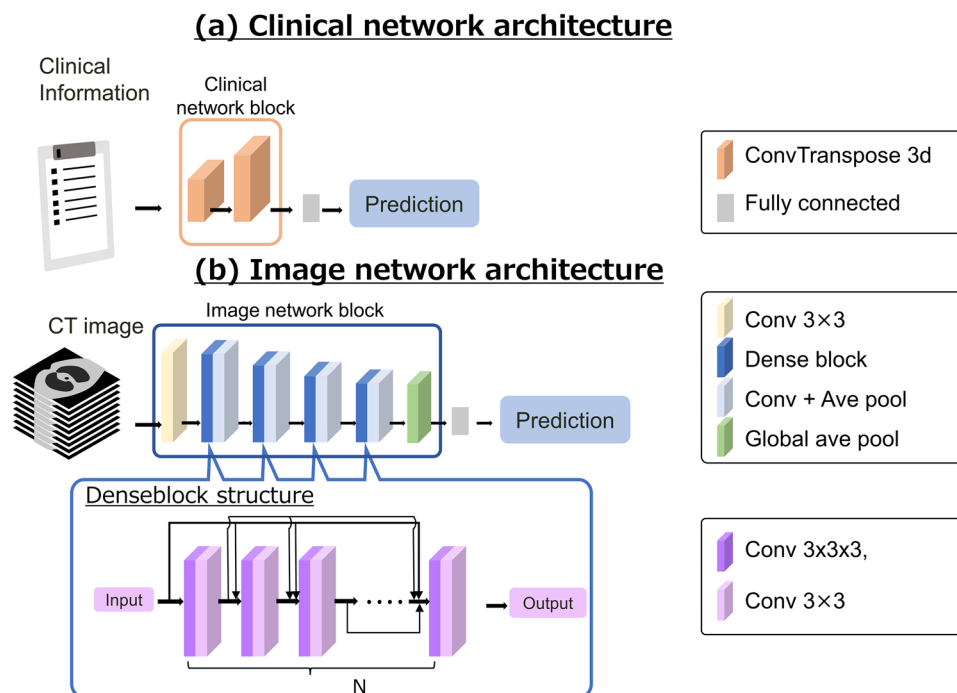

Fig. 1 Development of the DL models. Notes: The first DL model is the clinical network architecture, which is a DL model using clinical information (**a**). The clinical information (patient background, symptoms, and blood test findings; n = 62 items) was reformed into 62 channels, convo-transposed twice, and passed through a fully connected layer to generate outputs (1 for oxygen supplementation; 0 for no oxygen supplementation). The second DL model is the image network architecture, referring to a previous report based on Densenet [22]. This model was implemented using chest CT images (**b**). After

passing through the convolution layer, the model passed through three transitions: dense block, convolution layer, and average pooling. Then, after going through global average pooling, the model passed through the fully connected layer to produce the output. In each dense block, each network layer has a tightly coupled structure consisting of a 3*3 convolutional layer and a 3*3*3 convolutional layer. These layers are N-connected and have a residual structure where the outputs of each layer are added together from behind

Fig. 2 Development of the proposed DL model and proposed network architecture. Notes: The third model combined the clinical network with the image network. The DL model is the proposed network architecture. The products from the clinical network and image network were combined and passed through a fully connected layer, then through Resnet structures, and finally through a fully connected layer. Then, the final output was generated
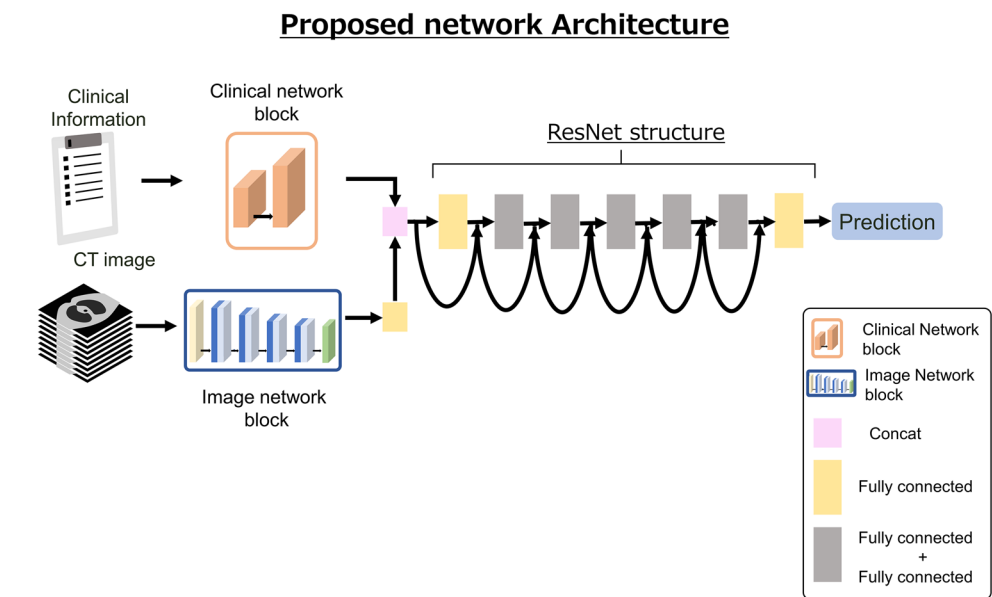
the learned model: I_p is the 3D chest CT image of patient $p(1 \leq p \leq P)$; and $C_{p1}, C_{p2} \cdots C_{pN}(N = 62)$ are the clinical items. $M(I_p, C_{p1}, \cdots C_{pn} \cdots, C_{pN})$ denotes the output (1 or 0) of the learned model to the input, $I_p, C_{p1}, \cdots C_{pn} \cdots, C_{pN}$.

The importance of the nth clinical item was defined as $Importance_n(\%)$.

$$Importance_n(\%) = \left(\frac{1}{P} \sum_p \left| M(I_p, C_{p1}, \cdots C_{pn} \cdots, C_{pN}) - M(I_p, C_{p1}, \cdots m_n, \cdots C_{pN}) \right| \right) \times 100,$$

Here, m_n represents the mean of P values in terms of the nth clinical item. The importance is the absolute value of the difference between the original estimate and the estimate obtained by inputting the value of the nth clinical item of each subject fixed at mean values (m_n) into the learned model and averaged over all patients. The importance of each of the 62 items was estimated for each of the original derivation and external evaluation data.

Statistical analysis

The results are expressed as the mean ± standard deviation (± SD). Categorical data are expressed as a number (%). All the statistical analyses were performed using JMP Pro version 17.0 software (SAS Institute, Cary, NC, USA). Differences between the three groups were evaluated by the Kruskal–Wallis test for data and comparisons between the two groups were performed using the Steel–Dwass method. We also calculated the areas under the receiver operating curve (AUC), accuracy, sensitivity, and specificity for the prediction of oxygen supplementation during the hospitalization. Model performance was quantified by the AUC and compared using Delong's test. A P value < 0.05 was considered significant.

Results

Characteristics of the study participants

The demographic participants are shown in Table 1. At the first facility, the average patient age was 52 years, males predominated, and the mean time interval from symptom onset to CT was 5.4 days. The chief symptom at the time of admission was fever for 86% of the patients, cough in 51%, dyspnea in 35%, fatigue in 46%, and dysgeusia or dysosmia in 26%.

A comparison between the first facility, and the first and 2nd external facilities showed differences in age and cigarette smoking status, etc. There were also differences in the proportion of subjects with hypertension, diabetes mellitus, and chronic obstructive pulmonary disease (COPD), and differences in clinical items, such as dyspnea, fatigue, sore throat and dysgeusia or dysosmia.

Table 1 Demographics of the study subjects (n = 738, 191, 230)

	Original derivation (n = 738) n (%, percentage)	1st External validation (n = 191) n (%, percentage)	2nd External validation (n = 230) n (%, percentage)
Age	52 (20–99)	58 (20–97) [†††]	62 (20–97) [‡‡‡, ***]
Gender (male)	444 (60%)	117 (61%)	128 (56%) [‡ **]
BMI	24.4 ± 4.6	24.8 ± 5.7	24.7 ± 4.6
Current smoker	218 (30%)	20 (10%) [†††]	35 (15%) [‡‡‡]
Pack-years	10.8 ± 20.3	7.5 ± 18.5 [†††]	13.7 ± 23.9 [***]
Alcohol consumption	381 (52%)	52 (28%) [†††]	N.A
Symptom onset to CT (days)	5.4 ± 4.7	5.9 ± 4.2	4.7 ± 3.5 [‡‡‡ ***]
Co-morbidities			
Hypertension	186 (25%)	74 (39%) [†††]	97 (42%) [‡‡‡]
Diabetes mellitus	96 (13%)	45 (24%) [†††]	52 (23%) [‡‡]
Dyslipidemia	90 (12%)	22 (12%)	44 (19%) [‡]
Coronary disease	15 (2%)	13 (7%) [††]	12 (5%) [*]
Bronchial asthma	37 (5%)	10 (5%)	11 (5%)
COPD	4 (0.5%)	9 (5%) [†††]	9 (4%) [‡‡‡]
Symptom			
Fever	633 (86%)	180 (94%) [††]	186 (81%) [***]
Cough	373 (51%)	84 (44%)	120 (52%)
Dyspnea	253 (35%)	102 (53%) [†††]	56 (24%) [‡****]
Fatigue	338 (46%)	39 (20%) [†††]	84 (37%) [‡****]
Sore throat	201 (27%)	26 (14%) [†††]	36 (16%) [‡‡‡]
Diarrhea	85 (12%)	14 (7%)	27 (12%)
Nausea/vomitting	50 (7%)	9 (5%)	4 (2%) [‡‡]
Dysgeusia/dysosmia	191 (26%)	8 (4.2%) [†††]	24 (10%) [‡‡‡*]
None	17 (2%)	2 (1%)	9 (4%)
Outcome			
Oxygen supplementation	250 (34%)	130 (68%) [†††]	97 (42%) [***]
Oxygen supplementation at time of hospital admission	35 (5%)	126 (66%) [†††]	62 (27%) [‡‡‡ ***]
High-flow nasal oxygen	79 (11%)	23 (12%)	12 (5%) [‡*]
Intubation	20 (3%)	15 (8%) [††]	16 (7%) [‡‡]
ECMO	2 (0.3%)	2 (1%)	4 (2%) [‡]
Survival/death	713 (97%)/ 25 (3%)	178(93%)/13 (7%)	219(95%)/11 (5%)

Data are expressed as the mean ± standard deviation

BMI body mass index; *COPD* chronic obstructive pulmonary disease; *ECMO* extracorporeal membrane oxygenation; *NA* not assessed

The difference between original derivation and the first external validation

[†]$p < 0.05$; [††], $p < 0.01$; [†††], $p < 0.001$

The difference between original derivation and the second external validation

[‡]$p < 0.05$; [‡‡], $p < 0.01$; [‡‡‡], $p < 0.001$

The difference between the first and second external validations

[*]$p < 0.05$; [**], $p < 0.01$; [***], $p < 0.001$

Outcome of the patients

At the first facility, the number of patients receiving oxygen during hospitalization was 250 (34%), and 35 (5%) were on oxygenation at the time of admission. The number of patients with high-flow nasal canula (HFNC) therapy was 79 (11%). Twenty patients (3%) were intubated. Two patients needed extracorporeal membrane oxygenation (ECMO). Twenty-five of the total number of patients did not survive (Table 1).

Comparisons between the three groups showed that the first facility and 2 external facilities differed in the

proportion of patients with oxygen supplementation (34%, 68%, and 42%, respectively). There were also differences in the proportion of patients receiving oxygen supplementation on admission (5%, 66%, and 27%, respectively). In contrast, there were no apparent differences in survival/death.

Major blood test findings of the patients

At the first facility, the aspartate aminotransferase (AST), lactate dehydrogenase (LDH), C-reactive protein (CRP), blood glucose, and D-dimer levels were slightly elevated compared to the normal ranges (Table 2).

Comparisons between the three groups of patients showed differences in the albumin (ALB) level, albumin:globulin ratio (AG ratio), white blood cell (WBC) count, peripheral compartment cell types (basophil (Baso), eosinophil (Eosino), neutrophil (Neutro)), and the prognostic nutritional index (PNI), etc.

Performance of the prediction model for oxygen supplementation

The prediction accuracy for oxygen supplementation from the first derivation is shown in Fig. 3(a). We used the combined method to predict oxygen supplementation. In Fig. 3(b), the AUC was 0.899, the accuracy was 0.861, the sensitivity was 0.805, and the specificity was 0.889. The AUC was statistically superior for the integrated model compared to the clinical information model, and for the integrated model compared to the image model (vs. clinical information; $p = 0.017$ and vs. image; $p = 0.007$, respectively).

Results of external facility data validations

To test model robustness, we tested model performance in two independent cohorts with different locations and populations, patient backgrounds, and levels of medical resources. Using the proposed method, as shown in Fig. 4, the AUC of the 1st external validation was 0.836 and the AUC of the 2nd external validation was 0.864. In the first external validation, there was a significant difference between the integrated and image models ($p = 0.0365$), while there was no significant difference between the integrated and clinical information models ($p = 0.3322$). In the second external validation, there was a significant difference between the integrated and clinical information models ($p = 0.0026$), while there was no significant difference between the integrated and image models ($p = 0.7017$).

Analysis of factors influencing oxygen supplementation prediction among clinical information

Factors influencing the prediction of oxygen supplementation in clinical information are shown in Fig. 5. With respect to patient background and clinical symptoms, the presence of dyspnea was the most significant contributor (Fig. 5(a)), while LDH was the most significant blood laboratory parameter contributor (Fig. 5(b)).

Discussion

In the present study we presented a DL prediction model for oxygen supplementation using clinical information and chest CT images in patients with COVID-19. Oxygen supplementation is one of the key factors determining the need for inpatient treatment; the AUC of the proposed model in the original facility was as high as 89.9%. Since the beginning of the pandemic, detailed integration of patient demographics and radiographic features has not been fully utilized. We have also enabled visualization of the elements on which the DL model was based.

Compared to the model built using clinical information and radiologic images separately, the model combining the two components had higher prediction accuracy. CT images and clinical information function separately as different detectors in the model. Because the patient's condition was assessed by clinical information consisting of patient background and blood test findings, and imaging findings in different ways, the combined model may have acted as a stronger detector and contributed to improved prediction accuracy. Blood test findings reflect a variety of multi-organ parameters, including systemic inflammation, the condition of various organs (such as kidney and liver function), blood glucose levels, and blood clotting markers. Blood testing findings also strongly reflect the condition of each patient at the time of the procedure and have been used for the prediction of COVID-19 severity [32, 33].

In contrast, CT imaging mainly evaluates lung findings, which have numerous imaging characteristics. It takes time for pneumonia to become established after infection, and each image has normal and abnormal areas, as well as areas of improvement and exacerbation that reflect not only the condition at the time of the procedure, but also longitudinal changes [34, 35]. Therefore, the model combining clinical information and CT images may have contributed to improvement in prediction accuracy.

The model in the present study was relatively simple, requiring only a combination of clinical findings available in an exam room and CT images in order to predict a

Table 2 Major blood test findings of the study subjects (n = 738, 191, 230)

Laboratory indices	Original derivation	1st External validation	2nd External validation
TP (g/dL)	7.1 ± 0.6	$6.7 \pm 0.6^{\dagger\dagger\dagger}$	$6.8 \pm 0.5^{\ddagger\ddagger\ddagger\,*}$
ALB (g/dL)	4.0 ± 0.6	$3.4 \pm 0.6^{\dagger\dagger\dagger}$	$3.7 \pm 0.6^{\ddagger\ddagger\ddagger***}$
AG ratio	1.3 ± 0.3	$1.1 \pm 0.3^{\dagger\dagger\dagger}$	$1.2 \pm 0.3^{\ddagger\ddagger\ddagger***}$
AST (IU/L)	40.6 ± 34.0	$51.6 \pm 43.9^{\dagger\dagger\dagger}$	$41.1 \pm 36.7^{\ddagger\ddagger\ddagger}$
ALT (IU/L)	37.7 ± 41.2	42.6 ± 40.9	$33.9 \pm 28.0^{*}$
LDH (U/dL)	295.5 ± 146.3	$368.3 \pm 180.2^{\dagger\dagger\dagger}$	$282.1 \pm 152.7^{***}$
T-Bil (mg/dL)	0.69 ± 0.34	$0.61 \pm 0.33^{\dagger}$	$0.69 \pm 0.32^{**}$
γ-GTP (IU/L)	67.6 ± 104.7	$80.5 \pm 98.6^{\dagger\dagger\dagger}$	$56.3 \pm 75.2^{***}$
BUN (mg/dL)	14.9 ± 7.9	16.5 ± 9.6	$16.5 \pm 8.2^{\ddagger\ddagger}$
Cre (mg/dL)	0.84 ± 0.34	0.93 ± 0.97	0.92 ± 0.61
UA (mg/dL)	4.6 ± 1.6	4.8 ± 1.9	N.A
eGFR (ml/min/1.73 m^2)	77.2 ± 21.0	73.8 ± 24.9	$67.1 \pm 21.0^{\ddagger\ddagger\ddagger**}$
Na (mEq/L)	137.7 ± 3.8	$136.9 \pm 4.5^{\dagger}$	$138.4 \pm 3.6^{\ddagger***}$
K (mEq/L)	4.0 ± 0.4	4.0 ± 0.4	4.0 ± 0.4
Cl (mEq/L)	101.1 ± 4.2	$100.2 \pm 4.8^{\dagger}$	$101.4 \pm 3.7^{**}$
CPK (U/L)	195.4 ± 873.5	$281.1 \pm 1068.2^{\dagger\dagger\dagger}$	$270.2 \pm 1074.6^{*}$
CRP (mg/dL)	4.0 ± 4.8	$6.8 \pm 6.7^{\dagger\dagger\dagger}$	$4.5 \pm 5.5^{\ddagger\ddagger\ddagger}$
GLU (mg/dL)	124.0 ± 47.0	$141.0 \pm 58.9^{\dagger\dagger\dagger}$	$132.3 \pm 47.6^{\ddagger\ddagger\ddagger}$
WBC count (/μL)	5353 ± 2252	$6071 \pm 3254^{\dagger\dagger\dagger}$	$5373 \pm 2179^{\ddagger\ddagger\ddagger***}$
RBC count (×10^4/μL)	476.8 ± 59.9	463.1 ± 71.3	463.3 ± 70.9
HGB (g/dL)	14.4 ± 1.8	14.1 ± 2.1	14.0 ± 2.1
Hct (%)	41.9 ± 4.8	41.4 ± 5.7	40.9 ± 5.8
MCV (fL)	88.1 ± 5.3	$89.9 \pm 5.2^{\dagger\dagger}$	88.5 ± 5.4
MCH (pg)	30.2 ± 2.2	30.4 ± 2.0	30.3 ± 2.2
MCHC (%)	34.3 ± 1.3	$33.9 \pm 1.2^{\dagger\dagger\dagger}$	$34.2 \pm 1.2^{*}$
PLT (×10^4/μL)	20.4 ± 7.1	$18.8 \pm 7.4^{\dagger\dagger}$	$18.9 \pm 6.2^{\ddagger}$
Baso (%)	0.39 ± 0.37	$0.03 \pm 0.17^{\dagger\dagger\dagger}$	$0.28 \pm 0.27^{\ddagger\ddagger\ddagger***}$
Eosino (%)	0.98 ± 1.62	$0.40 \pm 1.88^{\dagger\dagger\dagger}$	$0.66 \pm 1.23^{\ddagger\ddagger\ddagger***}$
Neutro (%)	64.0 ± 18.8	$74.2 \pm 12.0^{\dagger\dagger\dagger}$	$68.7 \pm 13.8^{\ddagger\ddagger\ddagger***}$
Lympho (%)	23.7 ± 10.6	$19.3 \pm 10.0^{\dagger\dagger\dagger}$	$22.1 \pm 10.8^{*}$
Mono (%)	7.3 ± 3.3	$6.2 \pm 3.1^{\dagger\dagger\dagger}$	$7.4 \pm 3.5^{***}$
Neutro count (/μL)	3628 ± 1928	$4555 \pm 2367^{\dagger\dagger\dagger}$	$3847 \pm 2131^{\ddagger\ddagger\ddagger**}$
PNI	39.8 ± 6.7	$39.0 \pm 6.4^{\dagger\dagger}$	$42.0 \pm 6.8^{\ddagger\ddagger\ddagger***}$
D-dimer (ug/mL)	1.9 ± 10.9	4.2 ± 22.6	$1.6 \pm 4.2^{\ddagger\ddagger\ddagger}$

Data are expressed as the mean ± standard deviation

TP total protein; *ALB* albumin; *AG ratio* albumin:globulin ratio; *AST* aspartate aminotransferase; *ALT* alanine aminotransferase; *LDH* lactate dehydrogenase; *T-Bil* total bilirubin; *γ-GTP* γ-glutamyltransferase; *BUN* blood urea nitrogen; *Cre* creatinine; *UA* uric acid; *eGFR* estimated glomerular filtration rate; *Na* sodium; *K* potassium; *Cl* chloride ion; *CPK* creatine phosphokinase; *CRP* C-reactive protein; *GLU* glucose; *WBC* white blood cell; *RBC* red blood cell; *HGB* hemoglobin; *Hct* hematocrit; *MCV* mean corpuscular volume; *MCH* mean corpuscular hemoglobin; *MCHC* mean corpuscular hemoglobin concentration; *PLT* platelet; *Baso* basophil; *Eosino* eosinophil; *Neutro* neutrophil; *Lympho* lymphocyte; *Mono* monocyte; *PNI* prognostic nutritional index; *NA* not assessed

The difference between the original derivation and the first external validation

†p < 0.05; ††, p < 0.01; †††, p < 0.001

The difference between the original derivation and the second external validation

‡p < 0.05; ‡‡, p < 0.01; ‡‡‡, p < 0.001

The difference between the first and second external validations

*p < 0.05; **, p < 0.01; ***, p < 0.001

Fig. 3 Receiver operating characteristic (ROC) curve analysis of oxygen supplementation prediction by the DL model combined with clinical information and CT images. Notes: The prediction accuracy of the model combining clinical information and CT images was higher than that of clinical information and CT images alone. Green line; Clinical information. Thin blue line; CT image. Indigo line; Total data (Clinical information + CT image)

(a)

(b)
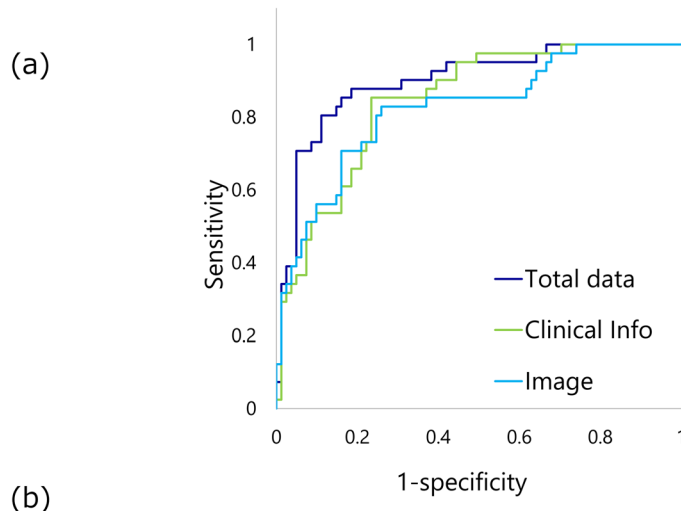
	AUC	Accuracy	Sensitivity	Specificity
Total data	**0.899**	**0.861**	0.805	**0.889**
Clinical info	0.846	0.795	**0.854**	0.765
Image	0.824	0.770	0.829	0.741

(a) 1st external validation
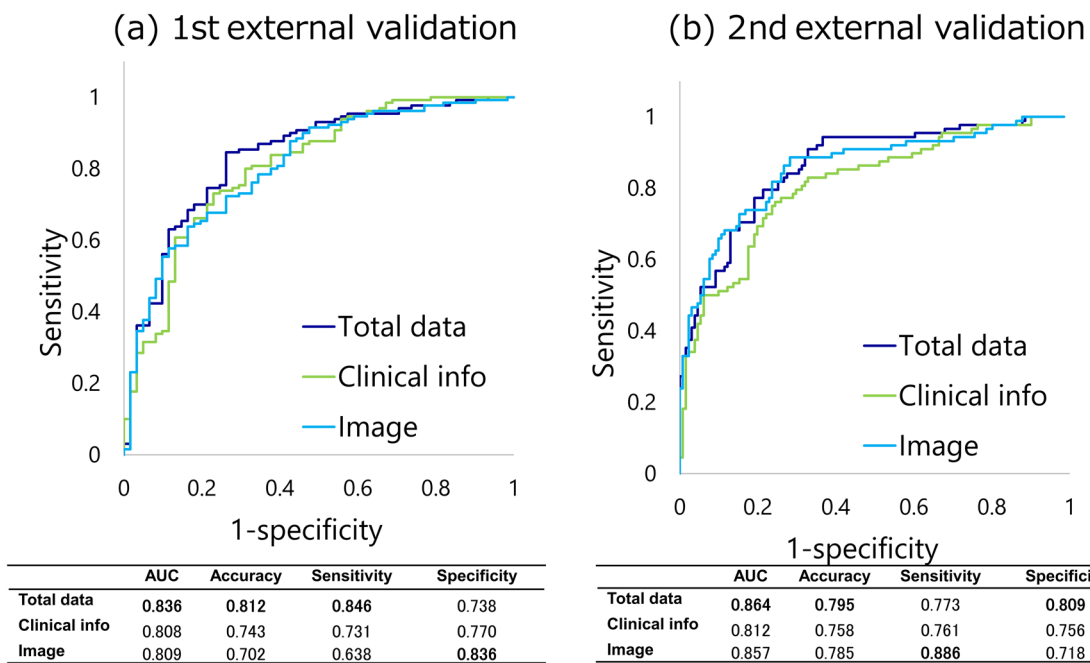
	AUC	Accuracy	Sensitivity	Specificity
Total data	**0.836**	**0.812**	**0.846**	0.738
Clinical info	0.808	0.743	0.731	0.770
Image	0.809	0.702	0.638	**0.836**

(b) 2nd external validation

	AUC	Accuracy	Sensitivity	Specificity
Total data	**0.864**	**0.795**	0.773	**0.809**
Clinical info	0.812	0.758	0.761	0.756
Image	0.857	0.785	**0.886**	0.718

Fig. 4 Receiver operating characteristic (ROC) curve analysis of oxygen supplementation prediction by the DL model combined with clinical information and CT images using externally-validated data. Notes: The validation results at the other two sites were > 80%. **a** and **b** First external validation. **c** and **d** Second external validation. Green line; Clinical information. Thin blue line; CT image. Indigo line; Total data (Clinical information + CT image)

patient's oxygen requirements. The proposed model combined DenseNet and ResNet, and integrated clinical information with CT images. Previous studies have used DL models, such as DenseNet-based models [22] and fully connected-based models [23] in COVID-19. Initially, with respect to the prediction of severe COVID-19 disease, there were limited reports from Japan, where the number of infected, severely ill, and critical cases was relatively small compared to the United States and other European countries; however, the increasing number of patients has caused a depletion
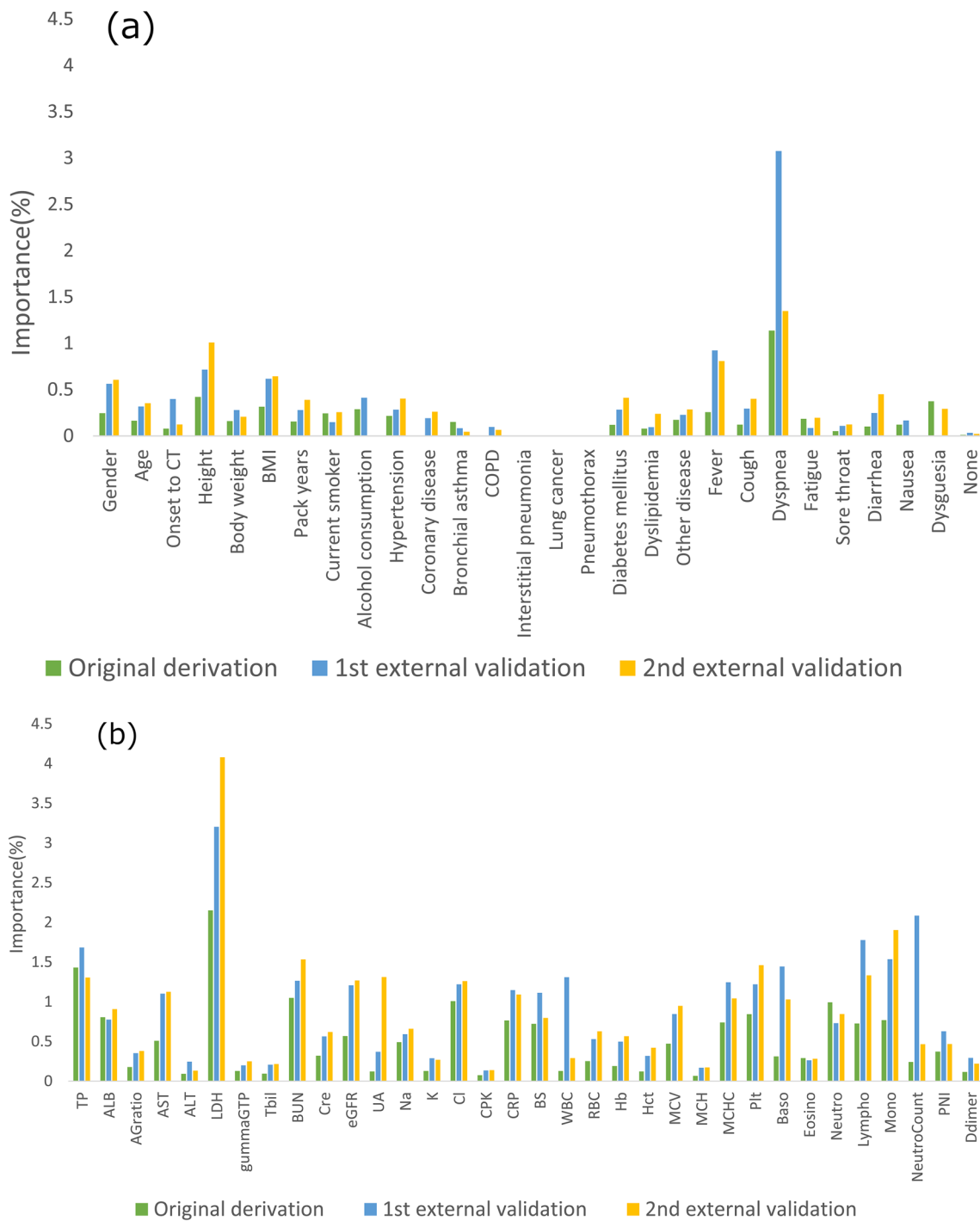
Fig. 5 Analysis of factors affecting oxygen supplementation prediction. Notes: Using the learned parameters, the importance of each item was evaluated by the proposed formula. Dyspnea, a clinical symptom, and LDH, a blood test finding, were shown to have a strong influence on the presence of oxygen supplementation. **a** The contribution of the items among patient background and clinical symptoms. **b** The contribution of the items among blood test findings. Abbreviations: *BMI* body mass index; *COPD* chronic obstructive pulmonary disease; *TP* total protein; *ALB* albumin; *AG ratio* albumin:globulin ratio; *AST* aspartate aminotransferase; *ALT* alanine aminotransferase; *LDH* lactate dehydrogenase; *T-Bil* total bilirubin; *γ-GTP* γ-glutamyltransferase; *BUN* blood urea nitrogen; *Cre* creatinine; *UA* uric acid; *eGFR* estimated glomerular filtration rate; *Na* sodium; *K* potassium; *Cl* chloride ion; *CPK* creatine phosphokinase; *CRP* C-reactive protein; *GLU* glucose; *WBC* white blood cell; *RBC* red blood cell; *HGB* hemoglobin; *Hct* hematocrit; *MCV* mean corpuscular volume; *MCH* mean corpuscular hemoglobin; *MCHC* mean corpuscular hemoglobin concentration; *PLT* platelet; *Baso* basophil; *Eosino* eosinophil; *Neutro* neutrophil; *Lympho* lymphocyte; *Mono* monocyte; *PNI* prognostic nutritional index

of medical resources that exceeded institution capacity. According to the COVID-19 Inpatient Registry in Japan (COVIREGI-JP), the breakdown of severity among 2638 patients with COVID-19 hospitalized in the early stages of the epidemic (March-July 2020) was as follows: no oxygen (62%), oxygen (30%), and ventilator therapy in intensive care (9%) [36, 37]. A similar trend was observed in the facilities where the proposed model was derived. The presence of oxygen supplementation is one of the key factors in determining the need for hospital admission and readiness for discharge. We believe that the proposed DL model can be used to properly identify patients in need of hospitalization, which may lead to appropriate use of healthcare resources.

In the current study, we tried to visualize the factors on which the DL model was based. Since the beginning of the pandemic, gender, age, obesity, and co-morbidities (e.g., diabetes, chronic respiratory disease, cardiovascular disease, chronic kidney disease, malignancy, and immuno-compromise immunity) have been reported as risk factors for severely ill patients [38]. In subsequent studies, blood tests have been reported to be predictive factors, such as CRP, erythrocyte sedimentation rate, granulocyte-lymphocyte ratio, KL-6, nutritional status, and elevated D-dimer [39–41]. In the present DL model, most of these factors were considered as clinical information inputs. As a method for evaluating the importance of the inputs to the DL estimation results, Grad-Cam for image input [42] and local interpretable model-agnostic (LIME) for table data [43] have been used in COVID-19. The analytic method for clarifying the contribution of methods that combine CT images and clinical information, such as the proposed DL model, has not been clarified. Therefore, we evaluated the importance of each item by the proposed formula using learned parameters. Dyspnea for clinical symptoms and LDH for blood tests were shown to strongly influence on the presence of oxygen supplementation. The high level of serum lactate dehydrogenase (LDH) and the presence of dyspnea have been reported to contribute to adverse outcomes in critically ill COVID-19 patients [44–46]. These two items reflect the severity and progression of SARS-CoV-2 pneumonia. The results of contributors by the proposed DL model were consistent with previous clinical reports and could provide a clear rationale for a DL model.

In this study, the prediction accuracy was reasonable at two external sites other than the first site where the DL model was constructed. The original facility and two different external facilities differed in location, local population, medical resources, and hospital functions. Specifically, in the first external validation, the integrated model improved predictive performance over the image-only model, and in the second external validation, the integrated model improved predictive performance over the clinical information-only model. We demonstrated that models based on either clinical information or images may have unstable accuracy due to the nature of the data, and suggested that integrating the two different types of data results in a more stable performance. We showed that a DL prediction model based on patient background, blood test findings, and radiologic features from one facility could be applied to other regional hospitals and outpatient clinics. To further improve the overall performance and consistency of the model, it is necessary to apply fine tuning with a small amount of data at each site. Recently, Menéndez et al. [47] created a nomogram for the severity score based on multi-center data from one surge, and showed that the results adapted to the following surges were acceptable. In the near future, our results will need to be further validated.

Numerous prognostic analyses using the DL model have been reported, especially in patients with malignant diseases [48], and many reports in COVID-19 also state that the DL model has improved the diagnostic performance of clinicians [14, 49]. The DL model proposed herein, which integrated clinical information with CT images, might be useful for the early prediction of disease severity in the next wave and for prediction of oxygen supplementation in other chronic respiratory diseases in the post-pandemic era, especially if the results can be incorporated into online entries in an examination room and electronic medical records.

This study had several limitations. First, this study was conducted as a retrospective study. Our data were obtained from a relatively small number of patients compared to general image recognition studies. Second, the internal validation showed an increase in prediction accuracy with models integrating clinical information and images. However, two external validations showed that the integrated model may not have sufficient generalization performance, with each integrated model showing only usefulness for one of the models. These results suggest that the integrated model may not be sufficiently robust to data features from different facilities. Further improvements in robustness and prediction accuracy are needed in the future, such as by increasing the number of data from other facilities in the training dataset, to improve generalization performance. Third, the duration of the study does not allow for detailed identification of the variant strain, although the type of variant strain can be estimated. In addition, patient vaccination status was not evaluated. Fourth, in the current retrospective study, it is possible that the decision to administer oxygen or not was based on careful judgement by the physician in charge especially when a patient with a chronic respiratory disease was asymptomatic or had a possible CO_2 narcosis. Prospective studies with uniform criteria will be needed in the near future. Fifth, a longitudinal data set, including treatment for

COVID-19, was not analyzed. We are conducting a corollary study to validate our model using longitudinal data, including hospitalized treatments. These preliminary results need to be confirmed in a larger multi-center longitudinal cohort.

Conclusion

The model's prediction accuracy in combining clinical information and CT images for oxygen supplementation was high. Deep learning-based severity prediction might be helpful in clinical practice in patients with COVID-19.

Declarations

References

1. WHO. Coronavirus disease (COVID-2019) situation reports.Coronavirus disease (COVID-2019) situation reports. World Health Organization; 2020. https://www.who.int/emergencies/diseases/novel-coronavirus-2019. (Accessed 8 Mar 2023).

2. Ranney ML, Griffeth V, Jha AK. Critical supply shortages—the need for ventilators and personal protective equipment during the Covid-19 pandemic. N Engl J Med. 2020;382:e41. https://doi.org/10.1056/NEJMp2006141.

3. Li Z, Yi Y, Luo X, Xiong N, Liu Y, Li S, et al. Development and clinical application of a rapid IgM-IgG combined antibody test for SARS-CoV-2 infection diagnosis. J Med Virol. 2020;92:1518–24. https://doi.org/10.1002/jmv.25727.

4. Zhang C, Zhou L, Liu H, Zhang S, Tian Y, Huo J, et al. Establishing a high sensitivity detection method for SARS-CoV-2 IgM/IgG and developing a clinical application of this method. Emerging Microb Infect. 2020;9:2020–9. https://doi.org/10.1080/22221751.2020.1811161.

5. Schneider J, Mijočević H, Ulm K, Ulm B, Weidlich S, Würstle S, et al. SARS-CoV-2 serology increases diagnostic accuracy in CT-suspected, PCR-negative COVID-19 patients during pandemic. Respir Res. 2021;22:119. https://doi.org/10.1186/s12931-021-01717-9.

6. Xu X, Yu C, Qu J, Zhang L, Jiang S, Huang D, et al. Imaging and clinical features of patients with 2019 novel coronavirus SARS-CoV-2. Eur J Nucl Med Mol Imaging. 2020;47:1275–80. https://doi.org/10.1007/s00259-020-04735-9.

7. Fang Y, Zhang H, Xie J, Lin M, Ying L, Pang P, et al. Sensitivity of chest CT for COVID-19: comparison to RT-PCR. Radiology. 2020;296:E115–7. https://doi.org/10.1148/radiol.2020200432.

8. Bernheim A, Mei X, Huang M, Yang Y, Fayad ZA, Zhang N, et al. Chest CT findings in coronavirus disease-19 (COVID-19): relationship to duration of infection. Radiology. 2020;295:200463. https://doi.org/10.1148/radiol.2020200463.

9. Ai T, Yang Z, Hou H, Zhan C, Chen C, Lv W, et al. Correlation of chest CT and RT-PCR testing for coronavirus disease 2019 (COVID-19) in China: a report of 1014 cases. Radiology. 2020;296:E32-e40. https://doi.org/10.1148/radiol.2020200642.

10. Xie X, Zhong Z, Zhao W, Zheng C, Wang F, Liu J. Chest CT for typical coronavirus disease 2019 (COVID-19) pneumonia: relationship to negative RT-PCR testing. Radiology. 2020;296:E41–5. https://doi.org/10.1148/radiol.2020200343.

11. Kianzad A, Meijboom LJ, Nossent EJ, Roos E, Schurink B, Bonta PI, et al. COVID-19: histopathological correlates of imaging patterns on chest computed tomography. Respirology. 2021;26:869–77. https://doi.org/10.1111/resp.14101.

12. Malpani Dhoot N, Goenka U, Ghosh S, Jajodia S, Chand R, Majumdar S, et al. Assigning computed tomography involvement score in COVID-19 patients: prognosis prediction and impact on management. BJR Open. 2020;2:20200024. https://doi.org/10.1259/bjro.20200024.

13. Park B, Park J, Lim JK, Shin KM, Lee J, Seo H, et al. Prognostic implication of volumetric quantitative CT analysis in patients with COVID-19: a multicenter study in Daegu. Korea Korean J Radiol. 2020;21:1256–64. https://doi.org/10.3348/kjr.2020.0567.

14. Wang H, Wang L, Lee EH, Zheng J, Zhang W, Halabi S, et al. Decoding COVID-19 pneumonia: comparison of deep learning

and radiomics CT image signatures. Eur J Nucl Med Mol Imaging. 2021;48:1478–86. https://doi.org/10.1007/s00259-020-05075-4.

15. Grasselli G, Greco M, Zanella A, Albano G, Antonelli M, Bellani G, et al. Risk factors associated with mortality among patients with COVID-19 in intensive care units in Lombardy, Italy. JAMA Internal Med. 2020;180:1345–55. https://doi.org/10.1001/jamainternmed.2020.3539.

16. Gao YD, Ding M, Dong X, Zhang JJ, Kursat Azkur A, Azkur D, et al. Risk factors for severe and critically ill COVID-19 patients: a review. Allergy. 2021;76:428–55. https://doi.org/10.1111/all.14657.

17. Zheng Z, Peng F, Xu B, Zhao J, Liu H, Peng J, et al. Risk factors of critical & mortal COVID-19 cases: a systematic literature review and meta-analysis. J Infect. 2020;81:e16–25. https://doi.org/10.1016/j.jinf.2020.04.021.

18. Zhou F, Yu T, Du R, Fan G, Liu Y, Liu Z, et al. Clinical course and risk factors for mortality of adult inpatients with COVID-19 in Wuhan, China: a retrospective cohort study. Lancet (Lond, Engl). 2020;395:1054–62. https://doi.org/10.1016/s0140-6736(20)30566-3.

19. Eljilany I, Elzouki AN. D-Dimer, Fibrinogen, and IL-6 in COVID-19 patients with suspected venous thromboembolism: a narrative review. Vascular Health Risk Manag. 2020;16:455–62. https://doi.org/10.2147/vhrm.S280962.

20. Xue M, Zhang T, Chen H, Zeng Y, Lin R, Zhen Y, et al. Krebs Von den Lungen-6 as a predictive indicator for the risk of secondary pulmonary fibrosis and its reversibility in COVID-19 patients. Int J Biol Sci. 2021;17:1565–73. https://doi.org/10.7150/ijbs.58825.

21. Meng L, Dong D, Li L, Niu M, Bai Y, Wang M, et al. A deep learning prognosis model help alert for COVID-19 patients at high-risk of death: a multi-center study. IEEE J Biomed Health Inform. 2020;24:3576–84. https://doi.org/10.1109/jbhi.2020.3034296.

22. Wang S, Zha Y, Li W, Wu Q, Li X, Niu M, et al. A fully automatic deep learning system for COVID-19 diagnostic and prognostic analysis. Eur Respiratory J. 2020. https://doi.org/10.1183/13993003.00775-2020.

23. Liang W, Yao J, Chen A, Lv Q, Zanin M, Liu J, et al. Early triage of critically ill COVID-19 patients using deep learning. Nat Commun. 2020;11:3543. https://doi.org/10.1038/s41467-020-17280-8.

24. Jiao Z, Choi JW, Halsey K, Tran TML, Hsieh B, Wang D, et al. Prognostication of patients with COVID-19 using artificial intelligence based on chest x-rays and clinical data: a retrospective study. Lancet Digit Health. 2021;3:e286–94. https://doi.org/10.1016/s2589-7500(21)00039-x.

25. Pyrros A, Flanders AE, Rodríguez-Fernández JM, Chen A, Cole P, Wenzke D, et al. Predicting prolonged hospitalization and supplemental oxygenation in patients with COVID-19 infection from ambulatory chest radiographs using deep learning. Acad Radiol. 2021;28:1151–8. https://doi.org/10.1016/j.acra.2021.05.002.

26. 2020 Health and Labour Policy Promotion Survey Grant, Emerging and Re-emerging Infectious Diseases and Vaccination Policy Promotion Research Project, Research Regarding Clinical Measures in Preparation for Occurrence of Category I Infectious Disease Patients. Clinical Management of Patients with COVID-19. A guide for front-line healthcare workers. Version 9. https://www.mhlw.go.jp/content/000936655.pdf. (Accessed 8 Mar 2023).

27. Huang G, Liu Z, Pleiss G, Van Der Maaten L, Weinberger K. Convolutional networks with dense connectivity. IEEE Trans Pattern Anal Mach Intell. 2019. https://doi.org/10.1109/tpami.2019.2918284.

28. Weiss K, Khoshgoftaar TM, Wang D. A survey of transfer learning. J Big Data. 2016;3:1–40.

29. He K, Zhang X, Ren S, Sun J. Deep Residual Learning for Image Recognition. arXiv preprint arXiv:1512.03385 (2015).

30. Selvaraju RR, Cogswell M, Das A, Vedantam R, Parikh D, Batra D. Grad-CAM: visual explanations from deep networks via gradient-based localization. IEEE International Conference on Computer Vision (ICCV). 2017;2017:618–26. https://doi.org/10.1109/ICCV.2017.74.

31. Roscher R, Bohn B, Duarte MF, Garcke J. Explainable machine learning for scientific insights and discoveries. IEEE Access. 2020;8:42200–16. https://doi.org/10.1109/ACCESS.2020.2976199.

32. Knight SR, Ho A, Pius R, Buchan I, Carson G, Drake TM, et al. Risk stratification of patients admitted to hospital with covid-19 using the ISARIC WHO clinical characterisation protocol: development and validation of the 4C Mortality Score. BMJ (Clin Res ed). 2020;370:m3339. https://doi.org/10.1136/bmj.m3339.

33. Gupta RK, Harrison EM, Ho A, Docherty AB, Knight SR, van Smeden M, et al. Development and validation of the ISARIC 4C Deterioration model for adults hospitalised with COVID-19: a prospective cohort study. Lancet Respir Med. 2021;9:349–59. https://doi.org/10.1016/s2213-2600(20)30559-2.

34. Kong M, Yang H, Li X, Shen J, Xu X, Lv D. Evolution of chest CT manifestations of COVID-19: a longitudinal study. J Thorac Dis. 2020;12:4892–907. https://doi.org/10.21037/jtd-20-1363.

35. Pan F, Ye T, Sun P, Gui S, Liang B, Li L, et al. Time course of lung changes at chest CT during recovery from coronavirus disease 2019 (COVID-19). Radiology. 2020;295:715–21. https://doi.org/10.1148/radiol.2020200370.

36. Matsunaga N, Hayakawa K, Terada M, Ohtsu H, Asai Y, Tsuzuki S, et al. Clinical epidemiology of hospitalized patients with coronavirus disease 2019 (COVID-19) in Japan: report of the COVID-19 registry Japan. Clin Infect Dis. 2021;73:e3677–89. https://doi.org/10.1093/cid/ciaa1470.

37. Terada M, Ohtsu H, Saito S, Hayakawa K, Tsuzuki S, Asai Y, et al. Risk factors for severity on admission and the disease progression during hospitalisation in a large cohort of patients with COVID-19 in Japan. BMJ Open. 2021;11:e047007. https://doi.org/10.1136/bmjopen-2020-047007.

38. Centers for Disease Control and Prevention. Underlying medical conditions associated with higher risk for severe COVID-19: information for healthcare providers. 2022. Available at: https://www.cdc.gov/coronavirus/2019-ncov/hcp/clinical-care/underlyingconditions.html. Accessed 2 Sep 2022.

39. Tan C, Huang Y, Shi F, Tan K, Ma Q, Chen Y, et al. C-reactive protein correlates with computed tomographic findings and predicts severe COVID-19 early. J Med Virol. 2020;92:856–62. https://doi.org/10.1002/jmv.25871.

40. Wei W, Wu X, Jin C, Mu T, Gu G, Min M, et al. Predictive significance of the prognostic nutritional index (PNI) in patients with severe COVID-19. J Immunol Res. 2021;2021:9917302. https://doi.org/10.1155/2021/9917302.

41. Berger JS, Kunichoff D, Adhikari S, Ahuja T, Amoroso N, Aphinyanaphongs Y, et al. Prevalence and outcomes of D-dimer elevation in hospitalized patients with COVID-19. Arterioscler Thromb Vasc Biol. 2020;40:2539–47. https://doi.org/10.1161/atvbaha.120.314872.

42. Harmon SA, Sanford TH, Xu S, Turkbey EB, Roth H, Xu Z, et al. Artificial intelligence for the detection of COVID-19 pneumonia on chest CT using multinational datasets. Nat Commun. 2020;11:4080. https://doi.org/10.1038/s41467-020-17971-2.

43. Fuhrman JD, Gorre N, Hu Q, Li H, El Naqa I, Giger ML. A review of explainable and interpretable AI with applications in COVID-19 imaging. Med Phys. 2022;49:1–14. https://doi.org/10.1002/mp.15359.

44. Lv XT, Zhu YP, Cheng AG, Jin YX, Ding HB, Wang CY, et al. High serum lactate dehydrogenase and dyspnea: Positive predictors of adverse outcome in critical COVID-19 patients in Yichang. World

J Clin Cases. 2020;8:5535–46. https://doi.org/10.12998/wjcc.v8.i22.5535.

45. Lazar M, Barbu EC, Chitu CE, Tiliscan C, Stratan L, Arama SS, et al. Interstitial lung fibrosis following COVID-19 pneumonia. Diagnostics (Basel). 2022. https://doi.org/10.3390/diagnostics12082028.

46. Iwamura C, Hirahara K, Kiuchi M, Ikehara S, Azuma K, Shimada T, et al. Elevated Myl9 reflects the Myl9-containing microthrombi in SARS-CoV-2-induced lung exudative vasculitis and predicts COVID-19 severity. Proc Natl Acad Sci USA. 2022;119:e2203437119. https://doi.org/10.1073/pnas.2203437119.

47. Menéndez R, Méndez R, González-Jiménez P, Zalacain R, Ruiz LA, Serrano L, et al. Early recognition of low-risk SARS-CoV-2 pneumonia: a model validated with initial data and infectious diseases Society of America/ American Thoracic Society Minor Criteria. Chest. 2022. https://doi.org/10.1016/j.chest.2022.05.013.

48. Hamamoto R, Suvarna K, Yamada M, Kobayashi K, Shinkai N, Miyake M, et al. Application of artificial intelligence technology in oncology: towards the establishment of precision medicine. Cancers (Basel). 2020. https://doi.org/10.3390/cancers12123532.

49. Zhang K, Liu X, Shen J, Li Z, Sang Y, Wu X, et al. Clinically applicable AI system for accurate diagnosis, quantitative measurements, and prognosis of COVID-19 pneumonia using computed tomography. Cell. 2020;182:1360. https://doi.org/10.1016/j.cell.2020.08.029.

Authors and Affiliations

Naoko Kawata[1,2,3] · Yuma Iwao[4,5] · Yukiko Matsuura[6] · Masaki Suzuki[7] · Ryogo Ema[8] · Yuki Sekiguchi[2] · Hirotaka Sato[1,9] · Akira Nishiyama[10] · Masaru Nagayoshi[6] · Yasuo Takiguchi[6] · Takuji Suzuki[1] · Hideaki Haneishi[4]

✉ Naoko Kawata
  chumito_03@yahoo.co.jp

  Yuma Iwao
  yuma1360@gmail.com

  Yukiko Matsuura
  matsuyuki_future@yahoo.co.jp

  Masaki Suzuki
  sz.suzu.masa@gmail.com

  Ryogo Ema
  r_emerson80@yahoo.co.jp

  Yuki Sekiguchi
  y_sekiguchi@chiba-u.jp

  Hirotaka Sato
  h.sato1980@gmail.com

  Akira Nishiyama
  midoriotoko1982@gmail.com

  Masaru Nagayoshi
  nagayos05@yahoo.co.jp

  Yasuo Takiguchi
  takiguchiyasuo@yahoo.co.jp

  Takuji Suzuki
  suzutaku@chiba-u.jp

  Hideaki Haneishi
  haneishi@faculty.chiba-u.jp

1   Department of Respirology, Graduate School of Medicine, Chiba University, 1-8-1, Inohana, Chuo-ku, Chiba-shi, Chiba 260-8677, Japan

2   Graduate School of Science and Engineering, Chiba University, Chiba 263-8522, Japan

3   Medical Mycology Research Center (MMRC), Chiba University, Chiba 260-8673, Japan

4   Center for Frontier Medical Engineering, Chiba University, 1-33, Yayoi-cho, Inage-ku, Chiba-shi, Chiba 263-8522, Japan

5   Institute for Quantum Medical Science, National Institutes for Quantum Science and Technology, 4-9-1, Anagawa, Inage-ku, Chiba-shi, Chiba 263-8555, Japan

6   Department of Respiratory Medicine, Chiba Aoba Municipal Hospital, 1273-2 Aoba-cho, Chuo-ku, Chiba-shi, Chiba 260-0852, Japan

7   Department of Respirology, Kashiwa Kousei General Hospital, 617 Shikoda, Kashiwa-shi, Chiba 277-8551, Japan

8   Department of Respirology, Eastern Chiba Medical Center, 3-6-2, Okayamadai, Togane-shi, Chiba 283-8686, Japan

9   Department of Radiology, Soka Municipal Hospital, 2-21-1, Souka, Souka-shi, Saitama 340-8560, Japan

10 Department of Radiology, Chiba University Hospital, 1-8-1, Inohana, Chuo-ku, Chiba-shi, Chiba 260-8677, Japan